Journal of Energy Chemistry 25 (2016) 754–760

Contents lists available at ScienceDirect

Journal of Energy Chemistry

journal homepage: www.elsevier.com/locate/jechem

http://www.journals.elsevier.com/journal-of-energy-chemistry/

First assessment of Li_2O–Bi_2O_3 ceramic oxides for high temperature carbon dioxide capture☆

E. M. Briz-López[a], M. J. Ramírez-Moreno[b], I. C. Romero-Ibarra[c], C. Gómez-Yáñez[a], H. Pfeiffer[b], J. Ortiz-Landeros[a,*]

[a] Departamento de Ingeniería en Metalurgia y Materiales, Escuela Superior de Ingeniería Química e Industrias Extractivas, IPN, UPALM, Av. Instituto Politécnico Nacional s/n, CP 07738, México DF, Mexico

[b] Instituto de Investigaciones en Materiales, Universidad Nacional Autónoma de México, Circuito exterior s/n, Cd Universitaria, Del. Coyoacán, CP 04510, México DF, Mexico

[c] Unidad Profesional Interdisciplinaria en Ingeniería y Tecnologías Avanzadas, IPN, Av. Instituto Politécnico Nacional No. 2580, CP 07340, México DF, Mexico

ARTICLE INFO

Article history:
Received 19 February 2016
Revised 20 April 2016
Accepted 26 April 2016
Available online 16 May 2016

Keywords:
CO_2 capture
Li_7BiO_6
Lithium bismuthates
Thermal analysis

ABSTRACT

The capacity to capture CO_2 was determined in several stoichiometric compositions in the Li_2O–Bi_2O_3 system. The compounds (Li_7BiO_6, Li_5BiO_5, Li_3BiO_4 and $LiBiO_2$ phases) were synthesized via solid-state reaction and characterized by X-ray diffraction, scanning electron microscopy and N_2 adsorption techniques. The samples were heat-treated at temperatures from 40 to 750 °C under the CO_2 atmosphere to evaluate the carbonate formation, which is indicative of the capacity of CO_2 capture. Moreover, Li_7BiO_6 shows an excellent CO_2 capture capacity of 7.1 mmol/g, which is considerably higher than those of other previously reported ceramics. Li_7BiO_6 is able to react with CO_2 from 240 °C to approximately 660 °C showing a high kinetic reaction even at CO_2 partial pressure values as low as 0.05.

1. Introduction

Among the different greenhouse gases, carbon dioxide (CO_2) is well known as the largest contributor to global warming [1]. In the last years, different lithium-containing ceramics have been proposed as possible CO_2 captors. Li_4SiO_4 [2–5], Li_2SiO_3 [6,7], Li_2CuO_2 [8,9], $Li_6Zr_2O_7$ [10,11], Li_4TiO_4 [12], Li_5AlO_4 [13,14] and Li_8SiO_6 [15,16] are all examples of ceramic sorbents with interesting capture properties from the point of view of high CO_2 capture capacities, high carbonation reaction rates at elevated temperatures and in some cases, good stabilities and cyclic properties. The post-combustion capture of CO_2 can be a more specific application for lithium ceramics [17,18].

For example, lithium orthosilicate (Li_4SiO_4), which is the most studied absorbent so far, shows a theoretical capacity to capture CO_2 (8.3 mmol/g) and it can operate in a wide range of temperature and CO_2 partial pressure (P_{CO2}). In fact, Li_4SiO_4 is able to react with CO_2 from room temperature to approximately 715 °C at low P_{CO2} values [2,3,19,20]. Li_4SiO_4 experiences carbonation through the reaction 1, and the trapping mechanism in this type of materials involves the reversible reaction on the ceramic oxide at high temperatures.

$$Li_4SiO_4 + CO_2 \leftrightarrow Li_2CO_3 + Li_2SiO_3 \quad (1)$$

The reaction shown in Eq. (1) (carbonation), starts at the surface of Li_4SiO_4 particles forming a shell of reaction products in a core-shell microstructure. The core, formed by unreacted Li_4SiO_4, reacts eventually with CO_2 diffused through the porous shell. In addition, Li^+ ions diffuse through the crystals from the core to the solid-gas interface to end up with the products shown in Eq. (1) [2,4]. Hence, the reaction 1 occurs through several processes. One strategy to increase the capture capacity of CO_2 could include the use of a ceramic where the processes involved in the carbonation reaction are improved. For example, the Li_7BiO_6 and Li_5BiO_5 phases have high theoretical CO_2 capture capacities, 9.4 and 7.7 mmol/g, respectively. Regarding ionic conductivity, these materials exhibit excellent lithium mobility over a wide temperature range [21,22]. Actually, Li_7BiO_6 and Li_5BiO_5 show conductivity values of 5.7×10^{-3} and 4.9×10^{-4} S/cm at 300 °C, respectively [23,24]. These values are significantly higher than those observed for other fast ionic conductors used as CO_2 captors [25]. As it was previously reported [26], due to the Li^+ ionic transport involved

☆ This work was supported by the SIP-IPN 20,151,545 Project. Furthermore, J. Ortiz-Landeros thanks to SIBE-IPN, and EDDI-IPN programs. I.C. Romero-Ibarra thanks to PICPAE-IPN program.

* Corresponding author. Tel: +52 5557296000x54267.
E-mail address: jortizla@ipn.mx (J. Ortiz-Landeros).

http://dx.doi.org/10.1016/j.jechem.2016.05.001

in the carbonation process, high carbonation kinetics might be expected for those materials exhibiting fast lithium mobility.

In this report, several compounds in the Li_2O–Bi_2O_3 were tested as CO_2 capture materials, looking for good capture capacities. The aim of this paper was to explore the potential use of lithium bismuthates in the capture of CO_2 at high temperature, and, at the same time, to analyze whether the mechanism of carbonation is similar or not to the reported previously for other lithium-containing ceramics as well as to establish the kinetic of the capture process.

2. Experimental

2.1. Preparation and characterization of lithium bismuthates

Li_2O–Bi_2O_3 ceramics were synthesized via solid-state reaction, using lithium oxide (Li_2O, Aldrich) and bismuth oxide (Bi_2O_3, Aldrich) as reagents. Specifically, Li_7BiO_6, Li_5BiO_5, Li_3BiO_4 and $LiBiO_3$ bismuthate samples were prepared. In all the synthesis, an excess of lithium oxide (5 wt%) was used to counteract the loss of lithium due to sublimation. Reactants were mechanically mixed using an agate mortar. Then, the mixed powder was uniaxially dry-pressed (5 ton/in^2) into disks with diameter of 15 mm and thickness of 2 mm. Pelletizing ensures the tight contact between the reactant particles and therefore promotes the solid state reaction. In all the cases, the obtained tablets were heat treated in a tubular furnace at 625 °C for 15 h under dry air. The used heating and air flow rates were 10 °C/min and 30 mL/min. Finally, the tablets were pulverized to further analysis of the powders.

Crystalline phase identification of the different samples was carried out by powder X-ray diffraction. XRD patterns were collected using a Bruker AXS diffractometer model D8 Focus equipped with a Cu *Kα* radiation source. The compounds were identified by the corresponding JCPDS files (Joint Committee Powder Diffraction Standards). The scanning electron microscopy (SEM) analysis was performed using an electronic microscope model JEOL JSM-6400 (MA, USA).

The specific surface area (SSA) of the Li_2O–Bi_2O_3 powders was measured by N_2 adsorption measurements using a Belsorp-mini II analyzer from BEL Japan. Samples were degassed at 90 °C for 12 h under vacuum prior to analysis. SSA values were obtained using the BET model.

2.2. CO_2 capture evaluation

The CO_2 capture capacity was evaluated by thermogravimetric analysis using a TA Instruments thermobalance model Q500-HR. The capture tests (dynamic and isothermal) were performed at temperatures between 40 and 750 °C. All the experiments were performed using a total CO_2 gas flow rate of 60 mL/min (Praxair, grade 3.0). Besides, to obtain the different isotherms, fresh samples were heated up to the target temperature under an inert atmosphere of N_2 (Praxair, grade 4.8). Then, once the experimental temperature conditions were reached, the gas was switched from N_2 to the reactive CO_2 gas. Additionally, the effect of CO_2 partial pressure (P_{CO2}) on the capture behavior of selected samples was evaluated. P_{CO2} values ranging from 0.05 to 1 were studied by feeding the thermobalance with the adequate CO_2–N_2 gas mixtures.

2.2.1. Cyclic CO_2 capture-regeneration evaluation

The stability of the material during cyclic carbonation–decarbonation processes was evaluated by thermogravimetric analysis. For the carbonation (capture), isothermal tests were performed at 570 °C during 45 min, using a total CO_2 gas flow rate of 60 mL/min. Then, for the decarbonation (regeneration) the atmosphere was switched from CO_2 to N_2 and the sample was heated up to 640 °C. Decarbonation process was conducted during 120 min, using a total N_2 gas flow rate of 60 mL/min. This cycle was repeated four times.

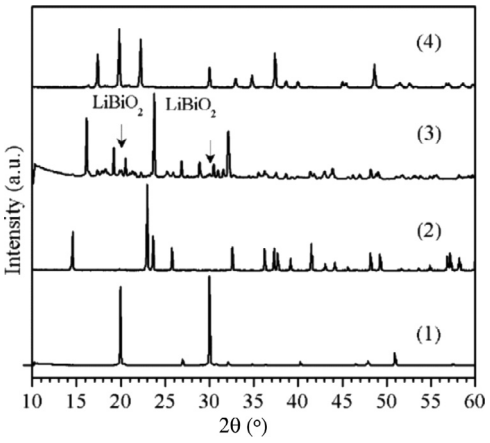

Fig. 1. XRD patterns of the different pristine lithium bismuthate phases. (1) $LiBiO_2$, JCPDS card No. 027-1221, (2) Li_3BiO_4, JCPDS card No. 018-0716, (3) Li_5BiO_5, JCPDS card No. 084-2002, (4) Li_7BiO_6, JCPDS card No. 026-841.

3. Results and discussion

3.1. Characterization of the samples and general analysis of the CO_2 capture process

Lithium bismuthates were successfully prepared via solid-state reaction method. Fig. 1 shows the XRD patterns of the different samples. The observed crystalline phases were identified by the corresponding JCPDS files. All of the samples but Li_5BiO_5 are pure. In this specific case, the presence of a minor secondary phase of $LiBiO_2$ was observed.

It is important to mention the obtaining of $LiBiO_2$ phase instead of $LiBiO_3$. The X-ray powder pattern of the obtained $LiBiO_2$ sample was fully identified with the card number 00-027-1221 (Fig. 1). It could be assumed that Bi^{3+} do not oxidize to Bi^{5+}, but another reason could be the thermal instability of $LiBiO_3$ at the used synthesis conditions; actually, it has been reported that $LiBiO_3$ converts to $LiBiO_2$ by releasing oxygen at temperatures above 300 °C [27].

Fig. 2 shows the SEM images of the synthesized compounds, including the Li_7BiO_6, Li_5BiO_5, Li_3BiO_4 and $LiBiO_2$ phases. In all the cases, the obtained powders are nonporous particles exhibiting irregular morphology. Powders are made of large micrometric particles (2–40 μm); the aforesaid microstructural features are typical of the lithium-containing ceramics that are prepared via solid state reaction method.

To elucidate the carbonation of lithium bismuthates and therefore the temperature range where the CO_2 capture takes place, a series of dynamic thermogravimetric tests were performed between 40 and 750 °C. Fig. 3 shows the thermogravimetric curves exhibiting the weight increase of the samples as a result of CO_2 capture from a 100 vol% CO_2 atmosphere. General speaking, all the samples show a weight gain at temperatures between 240 and about 660 °C. The weight decreases at higher temperatures ($T > 660$ °C). This behavior is attributed to the carbonation–decarbonation (regeneration) equilibrium temperature of these bismuthates and suggests the characteristic performance exhibited by other lithium-containing compounds during CO_2 capture [26]. Additionally, thermogravimetric curves show two different stages during carbonation; this behavior is observed for all the evaluated lithium bismuthates as follows. First, there is a moderate ini-

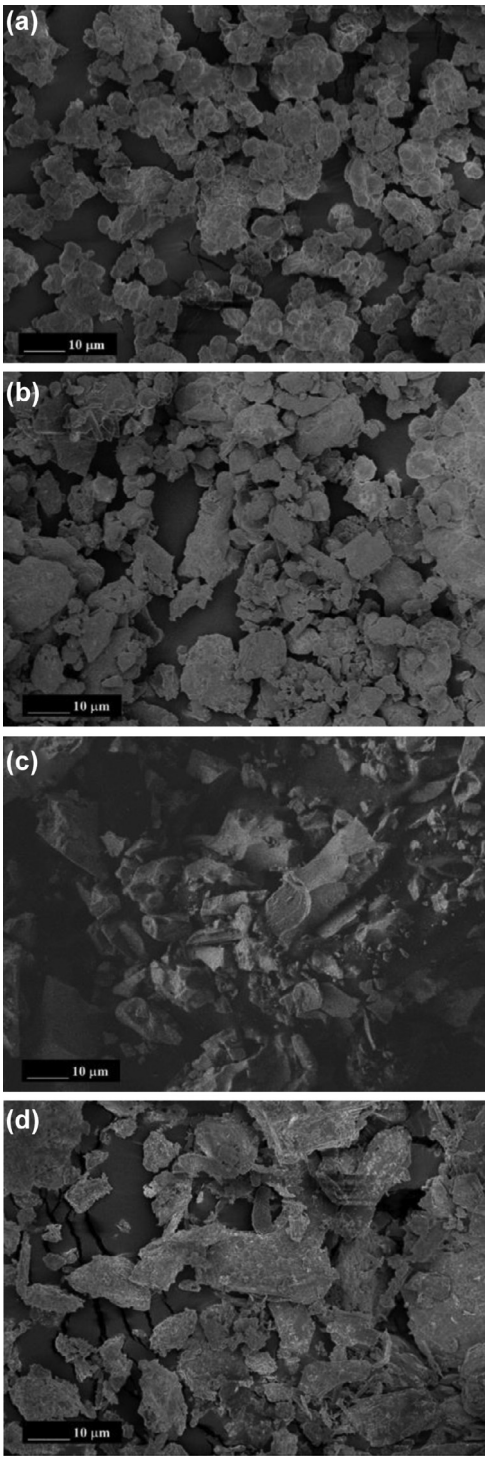

Fig. 2. SEM images of the different pristine lithium bismuthate phases: (a) Li_7BiO_6, (b) Li_5BiO_5, (c) Li_3BiO_4 and (d) $LiBiO_2$.

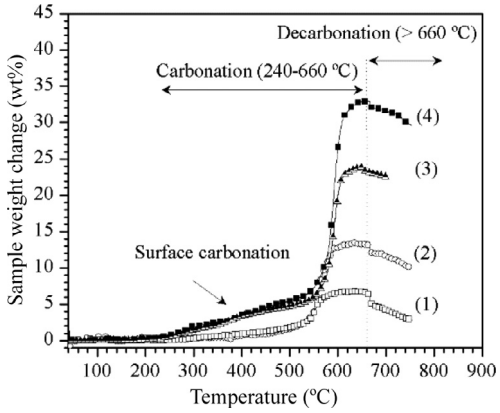

Fig. 3. Dynamic TG analysis of the Li_2O–Bi_2O_3 samples in a 100 vol% CO_2 flow. (1) $LiBiO_2$, (2) Li_3BiO_4, (3) Li_5BiO_5, (4) Li_7BiO_6.

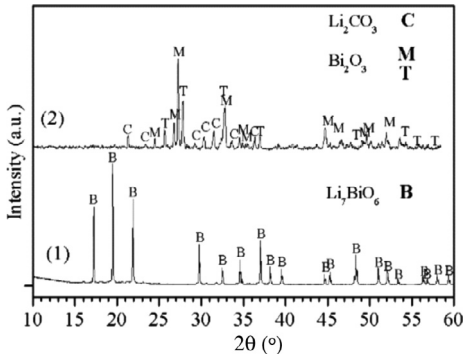

Fig. 4. XRD patterns of the pristine (1) and carbonated (2) Li_7BiO_6 samples. Crystalline phases are identified.

tial weight gain between 240 and about 540 ºC. In this range of temperature, samples show different carbonation degrees regardless of the total lithium content; actually $LiBiO_2$ exhibits the highest carbonation among the bismuthates. TG curve of $LiBiO_2$ shows a weight increase of 2 wt%, which is about 0.91 mmol/g or 24.2% of the theoretical CO_2 capture capacity of this material. On the contrary, the Li_7BiO_6, which is the sample with the highest Li:Bi ratio as well as the highest surface area of the series, only shows a weight increase corresponding to the 13.7% of the theoretical CO_2 capture capacity of the material (Table 1). Therefore, the observed behavior suggests certain differences about the reactivity of the materials at low temperature, probably due to the presence of different lithium amounts in surface which is prone to react with CO_2 to form Li_2CO_3.

In the second stage of the carbonation, all the samples present a remarkable weight gain between 540 and about 660 ºC. The maximum carbonation rate is observed in this stage that is related to the thermal activation of the Li^+ ionic conduction through the formed Li_2CO_3 phase [26]. Additionally, bismuthates clearly show certain differences regarding the maximum capture capacity, which is in agreement with their lithium contents. Table 1 shows the maximum CO_2 capture capacity observed during the dynamic thermogravimetric experiments.

Taking into consideration the carbonation reactions in Table 1, the final reaction products are Li_2CO_3 and Bi_2O_3. However, these ceramics may present only partial lithium release depending on temperature or other factors. In such a case, the external shell composition may change, as reported for Li_8SiO_6 [16]. The results obtained in the present paper, suggest that any lithium oxides (Li_5BiO_5, Li_3BiO_4, $LiBiO_2$) rather promote the subsequent carbonation reaction due to their observed reactivity properties (Fig. 3). This may be an important observation since the formation of secondary phases may or may not improve the further carbonation process [26].

All of the bismuthate samples were analyzed by XRD before and after the CO_2 capture process. The chemisorption products are mainly composed of the lithium carbonate (JCPDS card No. 22-1141) and a mixture of monoclinic (M) and tetragonal (T) crystalline bismuth oxide phases with JCPDS cards No. 41-1449 and No. 027-50, respectively. As an example, Fig. 4 shows the XRD patterns

Table 1. Capture properties of samples during heat up at 5 °C/min under a 100 vol% CO_2 atmosphere.

Material	Reaction	Theoretical CO_2 capture capacity (mmol/g)	Observed CO_2 capture from 240 to 520 °C (mmol/g)	Observed CO_2 capture at 660 °C (mmol/g)	Observed temperature of maximum absorption rate (°C)	SSA* (m^2/g)
Li_7BiO_6	$2Li_7BiO_6+7CO_2=7Li_2CO_3+Bi_2O_3+O_2$	9.4	1.29	7.1	591	1.10
Li_5BiO_5	$2Li_5BiO_5+5CO_2=5Li_2CO_3+Bi_2O_3+O_2$	7.7	1.13	5.4	589	0.55
Li_3BiO_4	$2Li_3BiO_4+3CO_2=3Li_2CO_3+Bi_2O_3+O_2$	5.1	0.45	3.1	560	0.23
$LiBiO_2$	$2LiBiO_2+CO_2=Li_2CO_3+Bi_2O_3$	3.8	0.91	1.5	552	0.21

* SSA_{BET}: values of the pristine bismuthate samples.

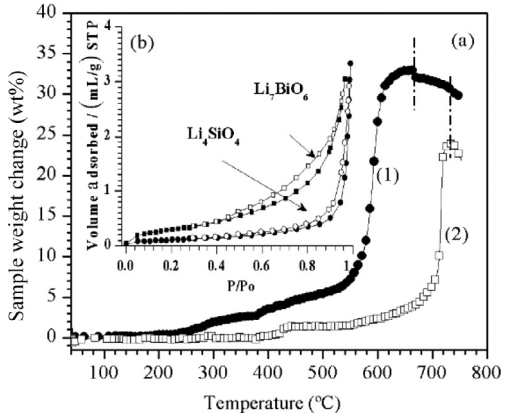

Fig. 5. (a) Comparative TG curves of the (1) Li_7BiO_6 and (2) Li_4SiO_4 samples in a 100 vol% CO_2 flow, and (b) inset shows the N_2 sorption isotherms.

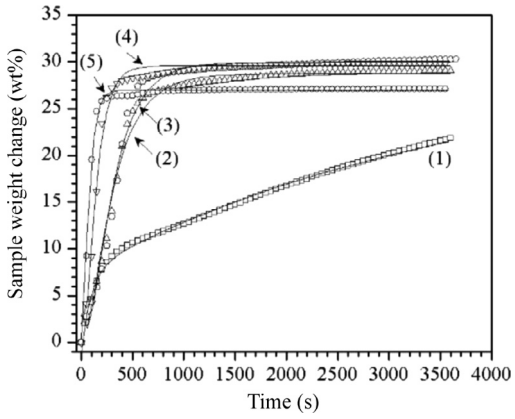

Fig. 6. Comparison of experimental TGA isotherms (symbols) and TG curves fitted to the double exponential model (solid curves). Isotherms of (1) 560 °C, (2) 580 °C, (3) 600 °C, (4) 620 °C, and (5) 640 °C.

of the pristine Li_7BiO_6 and the product powder after carbonation. In the Li_7BiO_6 carbonated product, the diffraction peaks assigned to Li_7BiO_6 disappear but those associated with Li_2CO_3 and Bi_2O_3 are observed. These results indicate that during the whole CO_2 chemisorption process, throughout the temperature range, Li_7BiO_6 reacts almost completely with CO_2.

The observed experimental CO_2 capture capacity of Li_7BiO_6 was estimated from the dynamic experiments as 7.1 mmol/g (Table 1). Therefore, the CO_2 absorption capacity of Li_7BiO_6 can be considered high among the previously reported lithium ceramics [2,12,17,18,26]. For example, Fig. 5 shows a comparative data of the dynamic carbonation tests performed on Li_7BiO_6 and Li_4SiO_4, where the later, is one of the most studied lithium-containing ceramics so far [2–5]. At low temperatures ($T < 520$ °C) both ceramics, Li_7BiO_6 and Li_4SiO_4 show a modest carbonation of 5.17% and 13.77% of their theoretical CO_2 capture capacities, respectively. The observed differences on the surface carbonation could be related with the specific surface area characteristics since lithium orthosilicate and the lithium bismuthate samples have SSA values of 0.4 and 1.1 m^2/g, respectively. Both materials show the N_2 adsorption isotherms type II which are typical of dense nonporous solids (Inset Fig. 5b) [28]. On the other hand, at higher temperature ($T > 520$ °C) the thermogravimetric curves show clear differences between the carbonation behaviors. Lithium bismuthate reaches a maximum chemisorption rate at lower temperatures (590–600 °C) than the lithium orthosilicate (690–720 °C). Additionally, Li_7BiO_6 exhibits a maximum weight increase of 32.9 wt% which is about 75.5% of its theoretical CO_2 capture capacity; on the contrary, the weight gain experienced by the Li_4SiO_4 sample (23.8 wt%) only corresponds to the 64.8% of the theoretical CO_2 capture capacity of the material. Here, it is important to point out that carbonation capacity is expressed based on the mass changes of the samples and therefore, the differences between the atomic weights of the metal structural elements, Bismuth (208.9 g/mol) and Silicon (28.08 g/mol), could mimic the real potential of this bismuthate. It is expected that the CO_2 chemisorption capacity of Li_7BiO_6 to be much higher as compared to Li_4SiO_4 and other CO_2 capture materials, since this bismuthate is able to release 7 lithium atoms per molecule to trap as much as 3.5 mol of CO_2 per mole of material. If the reaction 1 is considered, lithium orthosilicate only traps 1 mol of CO_2 per mole of material.

3.2. Analysis of CO_2 capture kinetics

To understand deeply the carbonation reaction kinetics in the Li_7BiO_6, different isothermal experiments were performed. Based on the dynamic TG analyses, the isothermal experiments were subsequently carried out in the temperature range from 560 to 640 °C. Fig. 6 shows the performed isothermal TG analyses. Despite the evident differences in the maximum weight gain as a function of the temperature, all the isotherms present the typical exponential behavior wherein the total weight increase could be split into two different steps that follow different reaction kinetics as well. First, considering short times, surface carbonation occurs and then isotherms show an exponential fast weight increase as a function of the time; on the other hand, at longer times the carbonation rate clearly slows down due to kinetics controlled by the diffusion processes.

In previous reports, the obtained isothermal thermogravimetric experimental data have been fitted to a double exponential model to describe the CO_2 capture on lithium-containing ceramics. Actually this mathematical model (Eq. (2)) has been used successfully to describe the carbonation behavior of several materials such as Li_4SiO_4 [3,29,32], $Li_6Zr_2O_7$ [10] and Li_5AlO_4 [13,14] among others.

$$W = A\exp^{-k_1 t} + B\exp^{-k_2 t} + C \quad (2)$$

where W represents the sample weight change due to CO_2 carbonation, t is the time, k_1 is the kinetic constant for the surface carbonation reaction and k_2 is the kinetic constant for the CO_2 capture once the carbonation is kinetically controlled by diffusion

Table 2. Carbonation reaction kinetic parameters of the Li_7BiO_6, Li_4SiO_4 [31,32] and Li_5AlO_4 [14] samples using the double exponential model.

	T (°C)	k_1 (1/s)	k_2 (1/s)	R^2
Li_7BiO_6				
	560	0.0106	0.0005	0.99
	580	0.0139	0.0040	0.98
	600	0.0171	0.0049	0.98
	620	0.0255	0.0099	0.98
	640	0.0518	0.0188	0.99
Li_4SiO_4				
Kinetic parameters reported by Zhang, et al. Ref. [31].				
	550	0.00407	0.00012	0.99
	575	0.00860	0.00014	0.99
	600	0.00851	0.00016	0.99
	650	0.00441	0.00026	0.99
	700	0.00198	0.00197	0.96
Li_4SiO_4				
Kinetic parameters reported by Wang, et al. Ref. [32].				
	550	0.00303	0.00025	0.99
	600	0.00431	0.00037	0.99
	650	0.00729	0.00046	0.99
	680	0.00879	0.00065	0.99
Li_5AlO_4				
Kinetic parameters reported by Ávalos-Rendón et al. Ref. [14].				
	500	0.00175	3×10^{-5}	–
	550	0.00153	8×10^{-5}	–
	600	0.00276	2.7×10^{-4}	–
	650	0.00257	2.7×10^{-4}	–
	675	0.00736	6.8×10^{-4}	–

processes. Additionally, the pre-exponential factors A and B indicate the range in which each process controls the whole reaction [10]. Isothermal TG curves were fitted to the Eq. (2) and the obtained k_1 and k_2 values are presented in Table 2. As expected, the reaction rate is increased by the temperature and the k_1 is one order of magnitude larger than k_2 which is in agreement with previous studies [3,14,29–32]. Therefore, the results suggest that diffusion processes (described by k_2) are the limiting step over the surface carbonation reaction (described by k_1). Besides, for comparative purposes, Table 2 shows the kinetic parameters previously reported by other authors for the CO_2 capture on Li_4SiO_4 and Li_5AlO_4 phases. The results show that Li_7BiO_6 has a significant higher rate for the carbonation reaction in the entire studied range of temperatures. First, the k_1 of lithium bismuthate is significantly higher than those observed for the surface carbonation of the Li_4SiO_4 [3,31,32] and Li_5AlO_4 [14] phases. This fact must be related with the reactivity of the material, and actually the lithium atom in the bismuthate crystal must be more weakly bonded than its counterpart in the case of the silicate and aluminate crystals.

Similar to k_1, in the case of lithium bismuthate, the k_2 values are at least one order the magnitude higher than those of other materials (Table 2). This fact must be related to the diffusional properties exhibited by the carbonation products layer. In the Li_7BiO_6, the products shell contains mainly Li_2CO_3 due to the high Li:Bi molar ratio in the material. In this sense, lithium carbonate has the ability to transport lithium ions through the crystal [26], as well as the ability to allow the transport CO_2 molecules through the interconnected porosity presenting whenever the temperature does not reach the carbonate sintering or melting values [33]. In order to elucidate the temperature dependency of carbonation kinetics, k_1 and k_2 constant values were fitted to Eyring's model. The linear form of the Eyring equation is as following:

$$\ln\left(\frac{k}{T}\right) = -\left(\frac{\Delta H^{\ddagger}}{R}\right)\left(\frac{1}{T}\right) + \ln\left(\frac{K_B}{h}\right) + \left(\frac{\Delta S^{\ddagger}}{R}\right) \quad (3)$$

where $\Delta H\ddagger$, $\Delta S\ddagger$ are the activation enthalpy and entropy respectively, and R is the universal gas constant. Then, it is clear that the obtained k values can be plot as $\ln(k/T)$ versus $1/T$ to calculate $\Delta H\ddagger$ from the slope (Fig. 7). The obtained $\Delta H\ddagger$ values for the surface carbonation and diffusion controlled carbonation process were 80.1 and 163.6 kJ/mol, respectively. Therefore, these results suggest that diffusion process rather depends on temperature than CO_2 surface carbonation in the case of Li_7BiO_6.

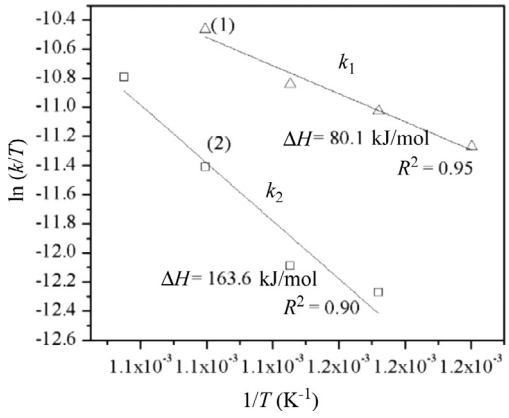

Fig. 7. Eyring's plot for the rate constants (1) chemisorption (k_1) and (2) diffusion (k_2) processes for Li_7BiO_6.

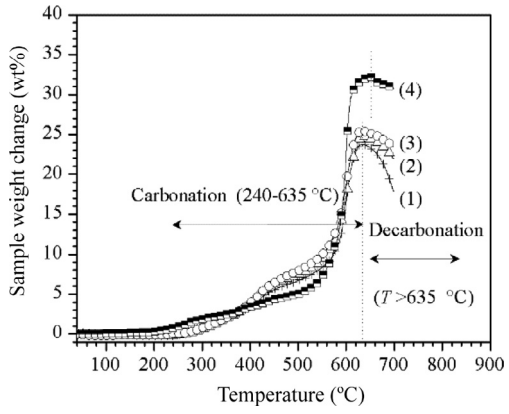

Fig. 8. TG analyses of the weight change of Li_7BiO_6 during high temperature carbonation at different P_{CO2} of (1) 0.05, (2) 0.1, (3) 0.2 and (4) 1.

3.3. Effect of CO_2 partial pressure on the carbonation behavior

Fig. 8 shows the weight change of the Li_7BiO_6 powder during heating from 40 to 750 °C at various CO_2 partial pressures. As mentioned, the increase and decrease of the sample weight on the TG curves are due to carbonation and regeneration respectively. Some differences are observed depending on the experimental conditions. At low P_{CO2}, the carbonation-regeneration temperature slightly shifts from 660 to 635 °C due to a change of the thermodynamic equilibrium. In addition, TG curves show a decrease on the observed experimental maximum of CO_2 capture when the P_{CO2} decreases. This behavior must be related with a change on the reaction kinetics; in fact, this phenomenon has been explained for the case of Li_4SiO_4 in terms of the CO_2 diffusional limitations through the formed product layer according to Fick's law [2].

A similar behavior has been previously reported for other materials [8,34]; for example, the Li_2ZrO_3 capture capacity decreases from 35.5% to 16.6% in the theoretical CO_2 capture capacity, when the carbonation dynamic experiments were performed at P_{CO2} values of 0.7 and 0.2, respectively. Therefore, in the present study, it is remarkable the fact that Li_7BiO_6 absorbent exhibits a high capture

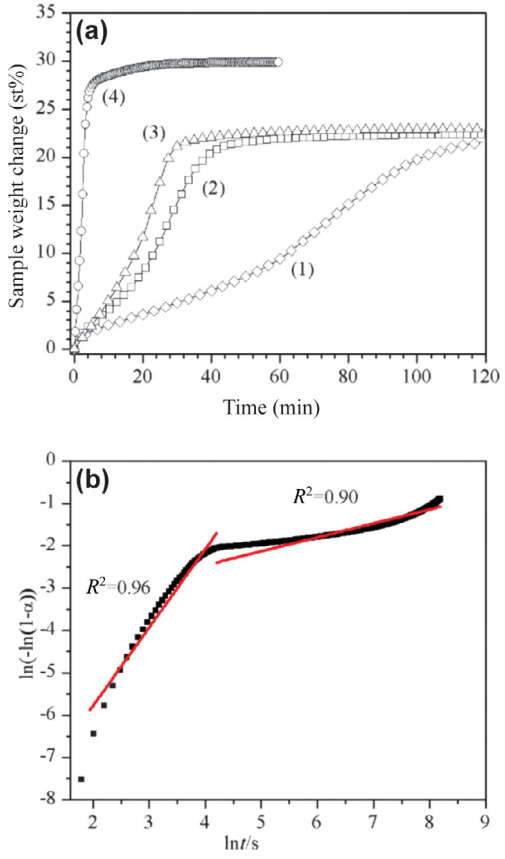

Fig. 9. (a) Isothermal TG curves of Li_7BiO_6 carbonation carried out at 620 °C under different CO_2 partial pressures of (1) 0.05, (2) 0.1, (3) 0.2 and (4) 1; and (b) ln(−ln(1−α)) versus ln*t* curve of the experimental data obtained for the isothermal test performed at P_{CO2} of 0.1.

capacity of 5.4 mmol/g even at P_{CO2} as low as 0.05 during dynamic experiments.

The observed effect of the CO_2 concentration on the carbonation reaction kinetics is in agreement with the results obtained by the isothermal TG analyses performed under different CO_2 partial pressures (Fig. 9a). In these series of experiments, Li_7BiO_6 experiences a weight gain of 26.8 wt% after 4.4 min of exposure to a P_{CO2} of 1 and 620 °C; subsequently, this sample reaches a maximum weight gain of 30.4 wt% after 60 minutes of carbonation. On the other hand, when Li_7BiO_6 reacts under a lower CO_2 partial pressure of 0.1, the material showed maximum weight increases of 22.5 wt% only after 120 min.

Selected isotherm was analyzed by applying the Avramy–Erofeev model, Eq. (4) [35]:

$$\ln(-\ln(1-\alpha)) = \ln k + n\ln t \quad (4)$$

Here $k = K^n$, and K is the kinetic constant, α is the degree of conversion, n is the kinetic parameter whose magnitude provides the

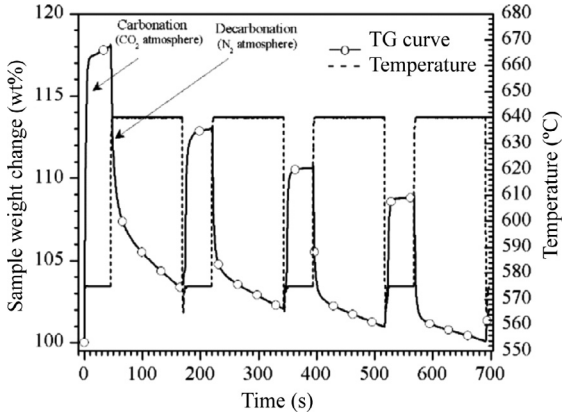

Fig. 10. Carbonation-regeneration cyclic test for Li_7BiO_6 in 100 vol% CO_2 (carbonation) and 100 vol% N_2 (decarbonation).

reaction rate which is controlled by the rate and growth of the carbonation products and *t* is the time [20,31].

Fig. 9(b) shows the ln(−ln(1−α)) versus ln*t* curve of the experimental data obtained for the isothermal carbonation test performed at 620 °C and P_{CO2} of 0.1. The curve clearly shows an inflexion point that suggests two different stages and therefore, splits the whole process into the rapid carbonation reaction stage and the diffusion-controlled stage [31]. Then, *n* and *K* parameters for the different stages were obtained by performing the corresponding linear fit. The obtained values are shown in Table 3.

As expected, the values of kinetic parameter *K* corresponding to the rapid reaction stage are much higher than that obtained for the diffusion control stage, which is in agreement with previous studies [20,31]. Besides, for comparative purposes, Table 3 shows the kinetic parameters *n* and *K* of the Avrami–Erofeev equation previously reported by other authors for the CO_2 capture on Li_4SiO_4 and K-doped Li_4SiO_4 phases. Once again, results show the higher reaction rates of the Li_7BiO_6 as compared to the Li_4SiO_4-based materials chosen as base line. Therefore, the superiority of the studied lithium containing bismuthates for CO_2 capture, in terms of capture capacity and reaction rate, is evident in this paper.

3.4. Analysis of the cyclic carbonation–decarbonation behavior

Finally, the regeneration ability of the Li_7BiO_6 was studied through four carbonation–decarbonation cyclic tests. The results are shown in Fig. 10, wherein solid and dotted lines denoted the weight change of the sample due to carbonation–decarbonation process and the temperature respectively. TG results suggest an incomplete regeneration of the material during decarbonation under the studied experimental conditions. Actually, it can be seen that sample experiences a gain of 18.2 wt% during the first carbonation cycle, however it only loses 14.6% during the subsequent decarbonation. Moreover, CO_2 capture efficiency decays from gradually after each successive capture-regeneration cycle. Taking into account the reversible carbonation–decarbonation reactions in Table 1, it could

Table 3. Parameters of Avrami–Erofeev model for the CO_2 capture process on Li_7BiO_6 and Li_4SiO_4 samples.

Sample	Temperature (°C)	CO_2 concentration (%)	Rapid reaction stage (surface carbonation)			Diffusion control stage			Ref.
			n	K/E^{-4}	R^2	*n*	K/E^{-7}	R^2	
Li_4SiO_4	575	100	1.86	26.4	0.98	0.36	15.10	0.99	[20]
Li_4SiO_4	575	10	1.10	0.48	0.93	0.27	0.38	0.95	[31]
K-doped	575	10	1.40	4.20	0.96	0.26	4.07	0.99	[31]
Li_7BiO_6	620	10	1.85	62.1	0.96	0.32	95.10	0.90	This work

be expected that regeneration of Li_7BiO_6 could be greatly enhanced under an oxygen containing atmosphere.

Because the capture-regeneration property is one of the most important factors that describes the quality of the lithium-containing CO_2 absorbents, it is important to mention that further studies must be performed towards understanding cyclic stability exhibited by the Li_7BiO_6. The CO_2 capture-regeneration process under specific operational conditions such as the presence of oxygen, water vapor and other gaseous species in the operational atmosphere should be addressed. Additionally, the structural and microstructural modification of the sorbents is others possible strategies to enhance even more the carbonation–decarbonation properties of this family of materials. Future work must be done in this sense.

4. Conclusions

The CO_2 capture properties of Li_2O–Bi_2O_3 ceramic oxides were demonstrated. Results suggest that these materials are able to capture CO_2 through the same mechanism of carbonation–decarbonation (regeneration) reported previously for other lithium-containing ceramics. Actually both, the double exponential and Avramy–Erofeev model were successfully used to describe carbonation process of Li_7BiO_6 absorbent wherein lithium diffusion is identified as the limiting step in the whole carbonation process.

Based on the experimental maximum capture capacity observed through the thermogravimetric analyses, the Li_7BiO_6 as well as the other studied lithium bismuthates would be considered as an interesting alternative for CO_2 capture in a wide range of temperatures (240–660 °C) and the evaluated CO_2 partial pressure values ($P_{CO2} = 0.05$–1).

Future work must be focused to enhance the capture-regeneration properties of these ceramic oxides towards the obtaining of new absorbent materials for a practical and more efficient CO_2 capture process.

References

[1] M.E. Boot-Handford, J.C. Abanades, E.J. Anthony, M.J. Blunt, S. Brandani, N. Mac Dowell, J.R. Fernández, M. Chiara Ferrari, R. Gross, J.P. Hallett, R.S. Haszeldine, P. Heptonstall, A. Lyngfelt, Z. Makuch, E. Mangano, R.T.J. Porter, M. Pourkashanian, G.T. Rochelle, N. Shah, J.G. Yao, P.S. Fennell, Energ. Environ. Sci. 7 (2014) 130–189.
[2] A. López-Ortiz, M.A. Escobedo-Bretado, V. Guzmán-Velderrain, M. Meléndez Zaragoza, J. Salinas-Gutiérrez, D. Lardizábal-Gutiérrez, V. Collins-Martínez, Int. J. Hydrogen Ener. 39 (2014) 16656–16666.
[3] H. Kima, H. Dong-Jang, M. Choi, Chem. Eng. J. 280 (2015) 132–137.
[4] M. Xiang, Y. Zhang, M. Hong, S. Liu, Y. Zhang, H. Liu, C. Gu, J. Mater. Sci. 50 (2015) 4698–4705.
[5] S.Y. Shana, Q.M. Jia, L.H. Jiang, Q. Chao Li, Y.M. Wang, J. Peng, Ceramics Int. 39 (2013) 5437–5441.
[6] J. Ortiz-Landeros, R. López-Juárez, I.C. Romero-Ibarra, H. Pfeiffer, H. Balmori-Ramírez, C. Gómez-Yáñez, Particuology 24 (2016) 129–137.
[7] J. Ortiz-Landeros, C. Gómez-Yáñez, H. Pfeiffer, J. Solid State Chem. 184 (2011) 2257–2262.
[8] K. Oh-ishi, Y. Matsukura, T. Okumura, Y. Matsunaga, R. Kobayashi, J. Solid State Chem. 211 (2014) 162–169.
[9] H.A. Lara-García, B. Alcántar-Vázquez, Y. Duan, H. Pfeiffer, RSC Adv., 5 (2015) 34157–34165.
[10] X.S. Yin, M. Song, Q.H. Zhang, J.G. Yu, Ind. Eng. Chem. Res. 49 (2010) 6593–6598.
[11] Y. Duan, J. Lekse, Phys. Chem. Chem. Phys. 17 (2015) 22543–22547.
[12] S. Ueda, R. Inoue, K. Sasaki, K. Wakuta, T. Ariyama, ISIJ Int., 51 (2011) 530–537.
[13] T. Avalos-Rendón, V.H. Lara, H. Pfeiffer, Ind. Eng. Chem Res. 51 (2012) 2622–2630.
[14] T. Ávalos-Rendón, J. Casa-Madrid, H. Pfeiffer, J. Phys. Chem. A 113 (2009) 6919–6923.
[15] P.R. Díaz-Herrera, M.J. Ramírez-Moreno, H. Pfeiffer, Chem. Eng. J. 264 (2015) 10–15.
[16] F. Durán-Muñoz, I.C. Romero-Ibarra, H. Pfeiffer, J. Mater. Chem. A 1 (2013) 3919–3925.
[17] S. Choi, J.H. Drese, C.W. Jones, ChemSusChem 2 (2009) 796–854.
[18] Q. Wang, J. Luo, Z. Zhong, A. Borgna, Ener. Environ. Sci. 4 (2011) 42–55.
[19] S.M. Amorim, M.D. Domenico, Tirzhá L.P. Dantas, H.J. José, R.F.P.M. Moreira, Chem. Eng. J. 283 (2016) 388–396.
[20] S. Zhang, Q. Zhang, H. Wang, Y. Ni, Z. Zhu, Int. J. Hydrogen Ener. 39 (2014) 17913–17920.
[21] C. Muhle, R.E. Dinnebier, L. van Wullen, G. Schwering, M. Jansen, Inorg. Chem. 43 (2004) 874–881.
[22] M. Wilkening, C. Muhle, M. Jansen, P. Heitjans, J. Phys. Chem. B Lett. 111 (2007) 8691–8694.
[23] E. Nomura, M. Greenblatt, J. Solid State Chem. 52 (1984) 91–93.
[24] C. Greaves, S.M.A. Katib, Mater. Res. Bull. 24 (1989) 973–980.
[25] V. Thangadurai, W. Weppner, Ionics 8 (3) (2002) 281–292.
[26] J. Ortiz-Landeros, T.L. Ávalos-Rendón, C. Gómez-Yáñez, J. Therm. Anal Calorim. 108 (2012) 647–655.
[27] N. Kumada, N. Takahashi, N. Kinomura, J. Solid State Chem. 126 (1996) 121–126.
[28] J. Rouquerol, F. Rouquerol, K. Sing, Adsorption by Powders and Porous Solids: Principles, Methodology and Applications, Academic Press, London, 1999.
[29] V.L. Mejía-Trejo, E. Fregoso-Israel, H. Pfeiffer, Chem. Mater. 20 (2008) 7171–7176.
[30] L. Martínez dlCruz, H. Pfeiffer, Ind. Eng. Chem. Res. 49 (2010) 9038–9042.
[31] Q. Zhang, D. Hand, Y. Liu, Q. Ye, Z. Zhu, AlChE J 59 (2013) 901–911.
[32] K. Wang, Z. Yin, P. Zhao, Ceram Int. 42 (2016) 2990–2999.
[33] L. Martinez-dlCruz, H. Pfeiffer, J. Phys. Chem. C 116 (2012) 9675–9680.
[34] K. Nakagawa, T. Ohashi, J. Electrochem. Soc. 145 (1998) 1344–1346.
[35] G.M. Zagorowsky, G.P. Prikhodḱo, V.M. Ogenko, G.K. Kovalćhuk, J. Therm. Anal. Calorim. 55 (1999) 699–705.